Desalination 586 (2024) 117840

Contents lists available at ScienceDirect

Desalination

journal homepage: www.elsevier.com/locate/desal

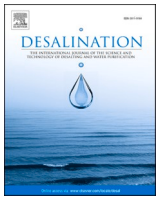

Experimental study on coalescer efficiency for liquid-liquid separation

Igor Matteo Carraretto *, Davide Scapinello, Riccardo Bellini, Riccardo Simonetti, Luca Molinaroli, Luigi Pietro Maria Colombo, Giampaolo Manzolini

Dipartimento di Energia, Politecnico di Milano, Via Lambruschini 4, Milano 20156, Italy

HIGHLIGHTS

- Experimental characterization of a liquid-liquid separator adopted in desalination.
- Coalescers efficiency evaluation for different draw temperatures and concentrations.
- Coalescer efficiency expression calibrated on the experimental outcomes.

ARTICLE INFO

Keywords:
Coalescer
Polymer
Regeneration
Draw agent
Forward osmosis
Desalination

ABSTRACT

The global community acknowledges water demand and accessibility as major challenges impacting human well-being. Forward Osmosis (FO) desalination coupled with concentrate solar power might represent a promising solution to combine water production with renewable sources. This work assesses the performance of a liquid-liquid separator (coalescer), an important component of the FO process, when using a polymeric thermo-responsive draw agent (PAGB2000). Experimental characterization of the coalescer is carried out for different regeneration temperatures (from 50 to 80 °C), residence time, draw concentration (from 0.30 to 0.60) and metal meshes. The separation efficiency of the coalescer can be as high as 95% for high residence time and regeneration temperatures (> 70 °C). Eventually, an analytical expression of the coalescer efficiency as function of the main operating parameters is proposed both to support desalination plant design and to enable understanding its applicability beyond its original context.

1. Introduction

The International Community has recognized water demand and accessibility as one of the most relevant challenges for the human well-being [1]. In response to the escalating demand, there is a pressing need to enhance the technologies employed in fresh-water production, striving for increased sustainability without compromising efficiency.

Desalination of seawater is an established technology to supply clean water where there is limited access to conventional water resources. It is expected that the energy consumptions in the desalination sector in 2040 will be six times higher than 2020, with an overall consumption of 345 TWh [2]. In the past, most of the desalination plants were based on Multi-Effect Distillation or Multi Stage Flash Technologies coupled with fossil fuel power stations [3], while recently membrane based processes have more than 80% of the market share [4]. To make desalination environmentally sustainable, the process should be coupled with renewable energy sources. The most obvious solution consists of coupling PV and RO taking advantage of the technology modularity and low cost [5]. Among the innovative processes, Forward Osmosis (FO) is one of the most promising in reason of its capability to exploit waste heat of Concentrated Solar Power (CSP) plants [6,7], therefore strongly reducing the energy cost to produce water.

The FO process is a membrane-based process where the driving force across the membrane is the osmotic pressure gradient between the seawater and the concentrated draw solution (DS) selected to be the higher-pressure side. This pressure disparity prompts the movement of water across the membrane, flowing from the less concentrated side to dilute the draw solute and equalize concentration levels. Concurrently, the solute or salt molecules present in the feed solution are selectively excluded or rejected [8]. The diluted DS requires additional treatment to separate the newly produced freshwater from the re-concentrated DS, enabling its reuse for subsequent dilution cycles. The absence of external hydraulic pressure requirements, coupled with benefits such as reduced membrane fouling and increased water recovery rates [9], contribute to the growing appeal of this emerging desalination technology. Up to now,

* Corresponding author.
E-mail address: igormatteo.carraretto@polimi.it (I.M. Carraretto).

https://doi.org/10.1016/j.desal.2024.117840
Received 25 March 2024; Received in revised form 20 May 2024; Accepted 11 June 2024
Available online 18 June 2024

Nomenclature

c	Mass concentration [kg/kg]
D	Coalescer inner diameter [m]
F	Volumetric flow rate [l/min]
L	Coalescer length [m]
n	Refractive index [brix]
T	Temperature [°C]
V	Coalescer volume [l]

Greek

ρ	Density [kg/m^3]
τ	Residence time [min]
ε	Efficiency [-]

Subscripts

exp	Experimental
in	Initial
M	Mesh
poor	Polymer-poor/water-rich branch
rich	Polymer-rich/water-poor branch
th	Theoretical

Acronyms

DS	Draw Solution
FO	Forward Osmosis
LCST	Lower Critical Solution Temperature
MARD	Mean Absolute Relative Deviation
MRD	Mean Relative Deviation
PV	Photo Voltaic
RO	Reverse Osmosis

researchers have mainly focused on studying the following crucial aspects: membranes, draw solutes and regeneration process.

Focusing on both the draw solutes and the regeneration process, keeping in mind that a low-cost regeneration of the diluted draw solution is required to make the process effective, it appears that a promising solution is to use a thermo-responsive draw agent [10] that can be regenerated by the rejected heat from the CO_2 power cycle integrated with a CSP plant (see Fig. 1). This is the idea behind the European Project DESOLINATION [11], where an advanced power cycle based on CO_2 blends releases heat at a temperature above 75 °C that is used in the regeneration step of the FO process [12,13]. Coupling the two technologies reduces installation costs making the produced electricity and water both competitive with other processes and CO_2 neutral [14,15].

On the other hand, turning our attention to the DS, different kinds of thermally regenerated DS are reported in the open literature. Zhang et al. [16] provides a comprehensive dissertation about the responsive mechanism, modified materials, modification methods, responsive capacity, FO performance and commercial feasibility of responsive DS. Focusing only on the most relevant ones, it is worth mentioning: (1) gas and volatile compounds [17], (2) phase transition materials [18,19] (such as lower/upper critical solution temperature (LCST [20]/UCST [21]) compounds, ionic liquids [22,23] and thermo-sensitive gels [24,25]), and (3) membrane distillations [26,27]. Phase transition materials exhibit unique phase behaviour, characterized by a temperature-dependent miscibility with water. In particular, regarding thermo-sensitive polymers, as the temperature is increased above the LCST, their long chain structures shrink and intertwine. Hence, the water molecules separate from the hydrophilic groups on the polymer's long chain structures, making the regeneration process easy [16].

In accordance with the analysis performed by Inada et al. [28,29], a LCST polymer can represent the best solution as draw agent guaranteeing both high osmotic pressure and simple regeneration process. However, both feasibility and effectiveness of the polymer regeneration process are two key aspects that have to be properly investigated in order to have an optimized plant design. According to the preliminary considerations reported in Colciaghi et al. [30], a coalescer is selected as key component to perform the regeneration process.

The coalescer is a static separator [31], mainly used in the petrochemical sector, able to separate two distinct immiscible solutions from a stable emulsion (liquid-liquid) or purify a gas from impurities to obtain high-quality gas (gas-liquid). The separator can be either vertically or horizontally positioned, in the latter circumstance the gravity force tends to increase the fluid residence time and hence its separation performances.

The concept of employing a coalescer gravity separator was in first instance presented by TREVI System [32] and then further investigated by Ahmed et al. [33]. In their work it is assessed the technical feasibility of using a thermo-responsive polyelectrolyte DS in a FO desalination pilot-scale system of 10 m^3/day capacity. Specifically, the study evaluates the effect of DS flow-rate and feed solution flow-rates on the net

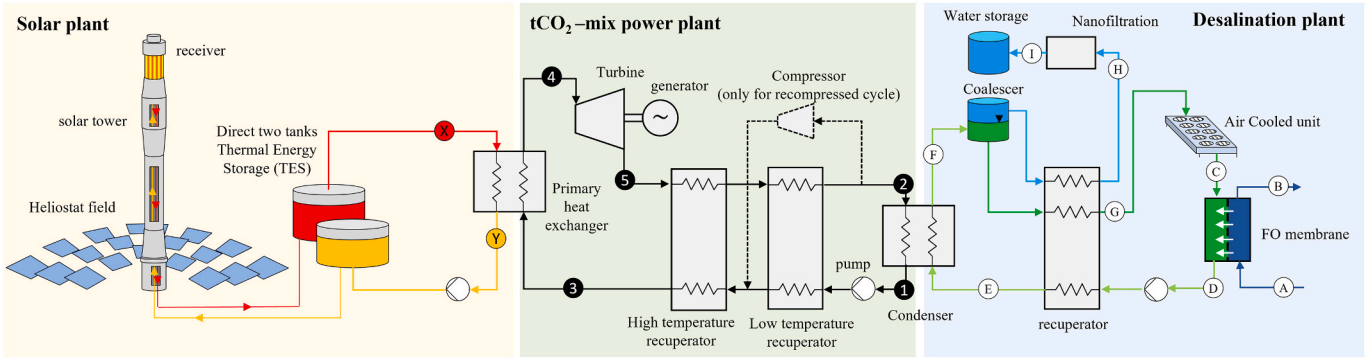

Fig. 1. Plant layout including: solar power (yellow box), power plant (green box) and desalination plant (blue box). (For interpretation of the references to colour in this figure legend, the reader is referred to the web version of this article.)

water recovery and product water flow-rates of the system. Eventually, the selected DS showed its potentiality towards the installation of commercial-scale FO desalination plant by witnessing its low viscosity and easy phase separation deploying a coalescer regeneration system that operates at a regeneration temperature of 85 °C.

Hence, due the scarcity in the open literature of both experimental and modelling results, an experimental campaign was performed with the aim of evaluating the performance of the coalescer to regenerate a thermo-responsive draw agent at various temperatures, flow rates and initial solution concentrations, intending to formulate an experimental expression of its efficiency. Having a formulation of the efficiency is, in first instance, crucial for both designing and sizing the nanofiltration section (see Fig. 1).

2. Experimental setup

2.1. Description of the test facility

The experimental facility (Fig. 2) is designed to reproduce the regeneration of the draw agent adopted in the FO plant (Fig. 1). The facility is designed to mimic the draw agent composition at the outlet of the membrane separator.

A tank (1), placed 1 m above the centrifugal pump (2) to prevent cavitation issues during operations, stores the aqueous solution at atmospheric pressure and at a temperature below the LCST one. A centrifugal pump is used to set the fluid flow-rate and to force it to pass through both the pre-heating (3) and the heating (4) sections. Three electric resistances (from 1.5 kW to 4 kW) are adopted to heat the draw solution to the regeneration temperature (T_{reg}). Subsequently, the fluid enters the coalescer (5) and the separation between the poor and rich phases occur. Within the coalescer a metal mesh is inserted to promote the coalescing process. The flow is then split in two different streams: (i) the polymer-rich phase that leaves the coalescer from the bottom, and (ii) the water-rich one that leaves the coalescer from the top. Each section has its own tap to collect samples of the stream. The two streams are then re-mixed and enter the hot side of the heat exchanger (3). Eventually, at the outlet of the heat exchanger, the fluid is cooled by an air cooler (6), before re-entering the storage tank (1).

As stated above, within the coalescer ($D = 0.20$ m, $L = 1.60$ m) three metal meshes are tested (Costacurta S.p.A.-VICO, Milano, Italy): (M1) STYLE42C, (M2) STYLE400, (M3) STYLE715; characterized by different mesh density (ρ_M): $\rho_{M1} = 262$ kg/m^3, $\rho_{M2} = 200$ kg/m^3, $\rho_{M3} = 190$ kg/m^3 (Fig. 3).

The thermo-responsive polymer is PAGB2000 whose thermo-physical characteristics are reported in [34] (see (Fig. 4) for LCST curve) and that has already been identified in previous studies as promising candidate in Forward Osmosis processes [28,30]. The polymer is known with the commercial name of UNILUBE 50MB-26, is produced by NOF Corporation (Tokyo, Japan) and used without further purification.

2.2. Measurement and instrumentation

In the experimental set-up, four thermo-resistances (RTD Pt100 IEC751 cl.A, Smeri, Assago (MI), Italy) are used to measure the temperatures and are located respectively at: (i) the inlet of the coalescer (T_{in}), (ii) the outlet of the coalescer on both branches (T_{rich} and T_{poor}), (iii) the outlet of the air cooler (T_{cooler}). Moreover, two flow-meters are used to measure the volumetric flow-rate and are located respectively at: (i) the outlet of the heat exchanger providing data on the total flow-rate (F) (PromagP300, 0–100 l/min, ±0.5% r.v., Endress Hauser, Reinach, Switzerland), (ii) at the outlet of polymer-poor (water-rich) branch (HTLD-MAG, 0–100 l/min, ±0.5% f.s., Smeri, Assago (MI), Italy) providing data on the water produced (F_{poor}). The polymer solution concentration measurement is performed using a portable refractometer (MA871, 0–85% *brix*, ±0.2%, Milwaukee, Rocky Mount (NC), United States), that provides the measurement of the refractive index (n [brix]). Hence, to obtain the weight concentration the following equation (retrieved from the calibration curve reported in Fig. 5) is applied:

$$c = \frac{101.68 - \sqrt{101.68^2 + 133.30(0.1 - n)}}{66.65}, \tag{1}$$

the uncertainty related to the measurement is computed according to:

$$u = \sqrt{\left(\frac{\partial c}{\partial n}\right)^2 I_n^2}. \tag{2}$$

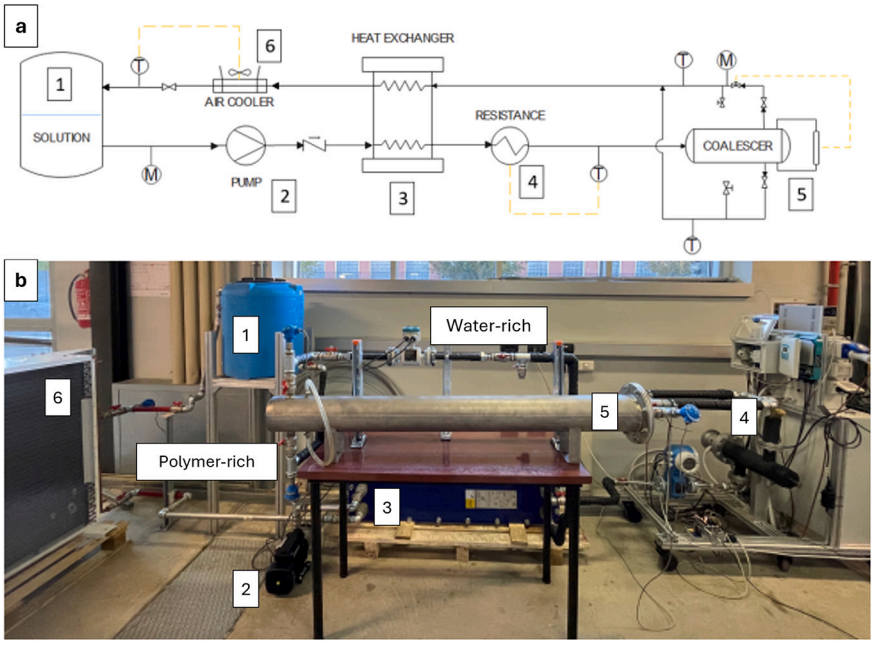

Fig. 2. (a) Experimental facility layout; (b) Experimental facility plant view.

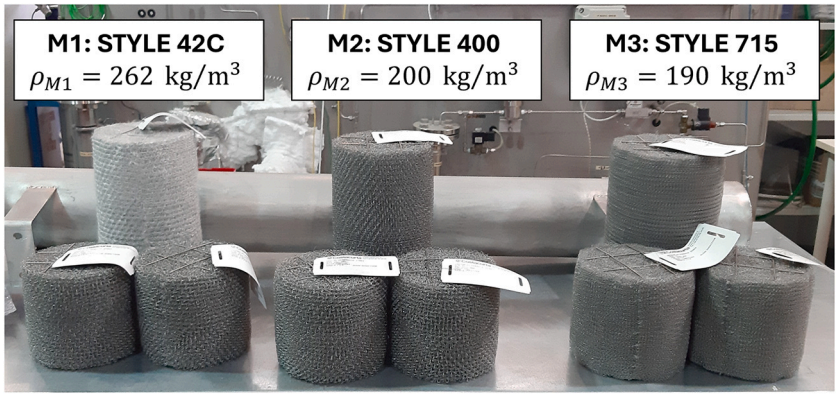

Fig. 3. Mesh tested during the experimental campaign.

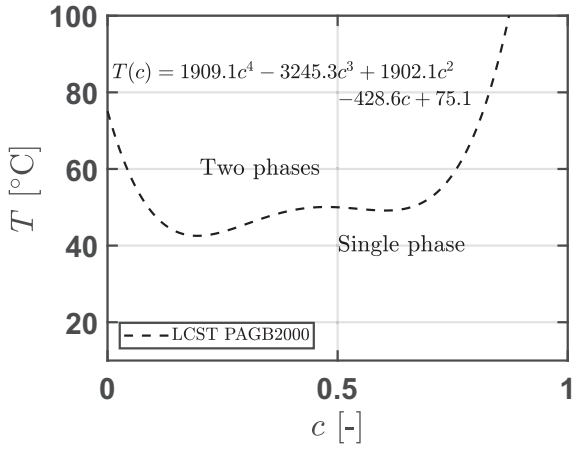

Fig. 4. Phase diagram of PAGB2000 reproduced from [34] with copyright permission from Elsevier.

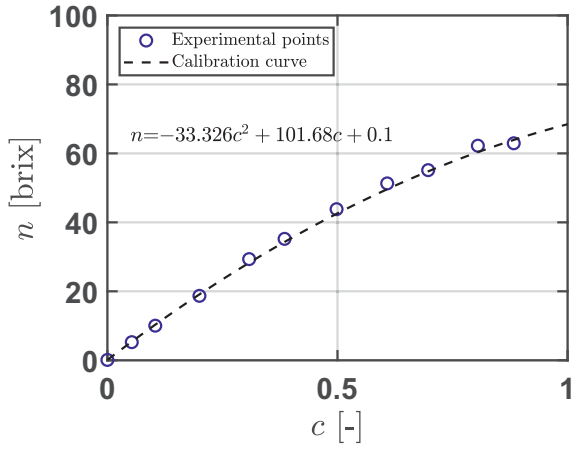

Fig. 5. Calibration curve to convert refractive index measured by the portable refractometer into weight concentration.

2.3. Operating conditions and testing procedure

The experimental conditions considered in this work are reported in Table 1. Overall, in the experimental campaign 3 meshes, 4 initial concentrations, 5 flow-rates and 6 regeneration temperatures are tested covering a broad range of operating conditions.

Table 1
Operating conditions investigated during the experimental campaign.

Mesh	c_{in} [−]	F [l/min]	T_{reg} [°C]
		4	60
	0.30	6	65
M1	0.40	8	70
M2	0.50	10	75
M3	0.60	12	80

The procedure implemented, starting from only-water tank, is here reported:

1. Add the amount of polymer required to obtain the desired concentration (wt./wt.);
2. Turn on the circulation pump to have a homogeneous concentration (approximately 20 min);
3. Check the concentration measuring the refractive index with the refractometer, 3 samples are extracted: storage tank, water-rich and polymer-rich branches;
4. Once the correct concentration is reached, set the flow-rate to the desired value;
5. Turn on and adjust the modular resistance to set the precise temperature value. Check that T_{in}, T_{rich} and T_{poor} are equal;
6. Adjust the flow-rate on the polymer-poor side (F_{poor}) using the valve placed at the coalescer output. F_{poor} has to be equal, within accuracy error, to a target value computed by the lever rule considering the T_{reg}, c_{in} and the *LCST* curve of the polymer;
7. Collect three samples of rich and poor solutions waiting 15 min between each sampling. On each sample three concentration measurements are performed;
8. Measure the refractive index three time once the samples are at 20 °C;
9. Modify either flow-rate or temperature and repeat (5–7), ensuring that T_{cooler} remains below 40 °C (i.e., lower than *LCST*) to guarantee a single-phase fluid at the beginning of the process for each initial tested concentration.

Due to technical issues, not all flow-rates are analysed at every temperature and measurements are not carried out. Specifically, the measurements are not performed at 4 l/min and 75 °C or 80 °C for safety reasons, as the low flow-rate is not high enough to prevent the overheating of the resistances. Moreover, the heating system is not able to guarantee the required steady-state conditions for both a flow-rate of 10 l/min and T_{reg} of 80 °C, and for a flow-rate of 12 l/min and T_{reg} of 75 °C and 80 °C. Besides these limitations, the number of experimental conditions allows to perform a solid analysis on the coalescer performances.

As stated in Section 1, the main objective of the experimental campaign is to find the influence of the regeneration temperature (T_{reg} [°C]), the initial fluid concentration (c_{in} [−]), and the residence time (τ [min]) on the coalescer separation efficiency. The residence time is calculated as the ratio between the coalescer volume and the total flow-rate.

2.4. Data reduction and analysis

The coalescer separation efficiency is defined as:

$$\varepsilon = \frac{c_{in} - c_{exp,poor}}{c_{in} - c_{th,poor}}, \tag{3}$$

representing the ability of the coalescer at approaching the concentration theoretically obtainable (using the phase diagram) with respect to the experimentally obtained one.

The modelling performance is checked, with respect to the experimental values, in terms of *MRD* and *MARD* defined as follows (where z_i is a generic quantity):

$$MRD = \frac{1}{N}\sum_{i=1}^{N}\frac{z_{i,exp} - z_{i,th}}{z_{i,exp}} \ (i) \text{ and } MARD = \frac{1}{N}\sum_{i=1}^{N}\frac{\left|z_{i,exp} - z_{i,th}\right|}{z_{i,exp}} \ (ii). \tag{4}$$

3. Experimental results and discussion

This section summarizes both the results of the experimental campaign and the characterization of the coalescer performance as function of the operating conditions. Firstly, the experimental characterization is presented, then the coalescer efficiency analysis is reported, and finally a generic expression, to be used when designing the coalescer, is introduced.

3.1. Concentration measurements

Considering the first mesh (M1) and the initial concentration of 0.50, the concentration results for the water-rich side (c_{poor}) as function of the total flow-rate and of the regeneration temperature are reported in Fig. 6.

The results show that the regeneration temperature is the most relevant parameter on achieving high-quality separated phases: at higher temperatures, the concentrations quickly approach the theoretical values (dashed lines in Fig. 6(a)). Nonetheless, a relevant role is also played by the flow rate/residence time: higher residence time (i.e., low flow-rate) favours the phase separation.

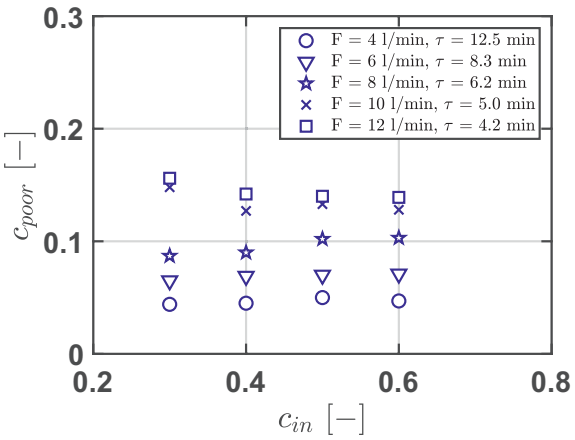

Fig. 7. Measured water-rich concentration (c_{poor}) vs. Initial concentration (c_{in}) for a fixed regeneration temperature of 60 °C and Mesh #1 (M1) at various flow-rates (F).

At last, the initial polymer concentration, for the four tested conditions, seems to play a marginal role within the separation process (Fig. 7).

The results of the experimental campaigns are synthetically reported in Figs. 8–10 in terms of water-rich (left-hand side of the charts) and polymer-rich (right-hand side of the charts) phases concentrations measured with respect to the LCST for the three meshes tested (more charts can be found in Appendix A where Figs. A.16 – A.18 report zoomed-in views on both the water-rich and polymer-rich branches for the three meshed at c_{in} = 0.50). Error bars representing measurement uncertainty are also included within the charts, always resulting in the range of ±0.002 to ±0.02.

As the initial concentration has limited impact on the process performance, only two conditions are plotted (i.e., 0.50 and 0.60) being the most likely to be used in the FO desalination plant.

It can be noted that the phase-separation is very close to the LCST curve in all the considered cases when a high regeneration temperature is considered (above 65 °C). These results indicate the very good performance of the separation process.

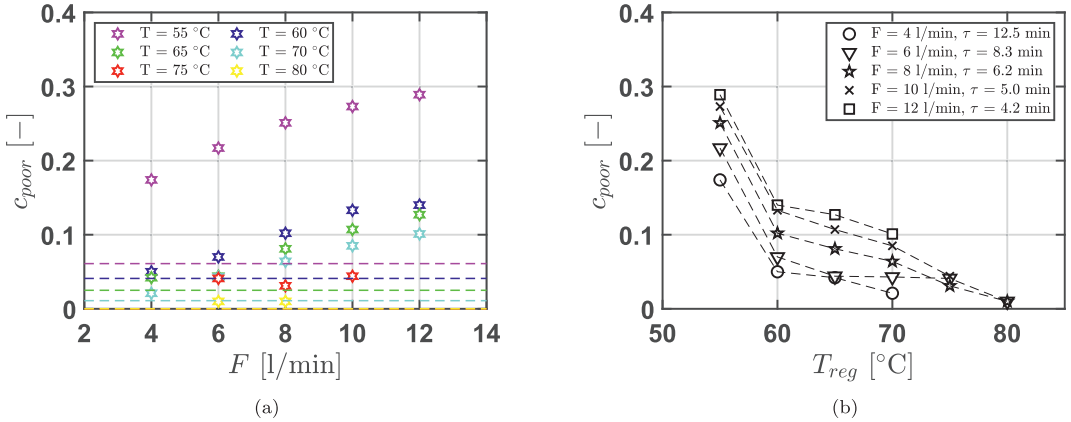

Fig. 6. Measured water-rich concentration (c_{poor}) for a fixed initial concentration (c_{in}) of 0.50 and Mesh #1 (M1) at: (a) different flow-rates (F); (b) regeneration temperatures (T_{reg}).

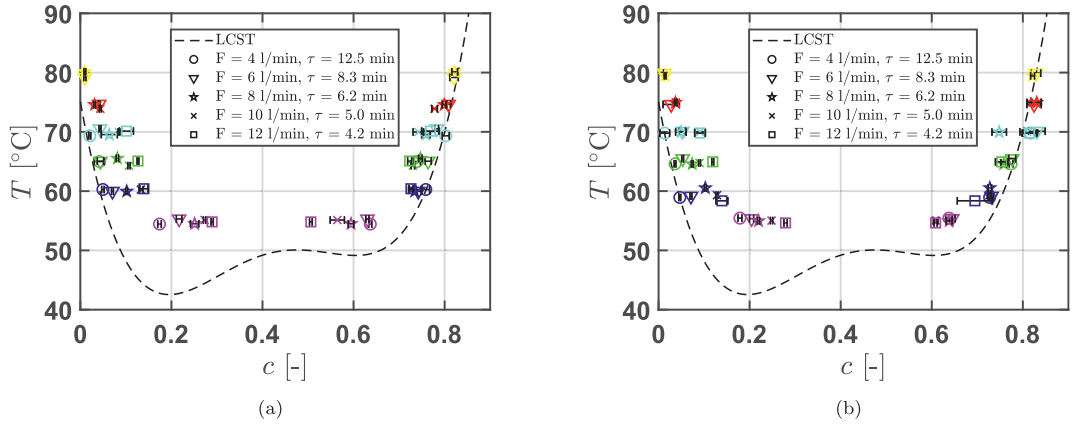

Fig. 8. Measured water-rich and polymer-rich phases concentrations compared with PAGB2000 LCST, at different T_{reg} and τ for Mesh #1 at: (a) c_{in} = 0.50; (b) c_{in} = 0.60.

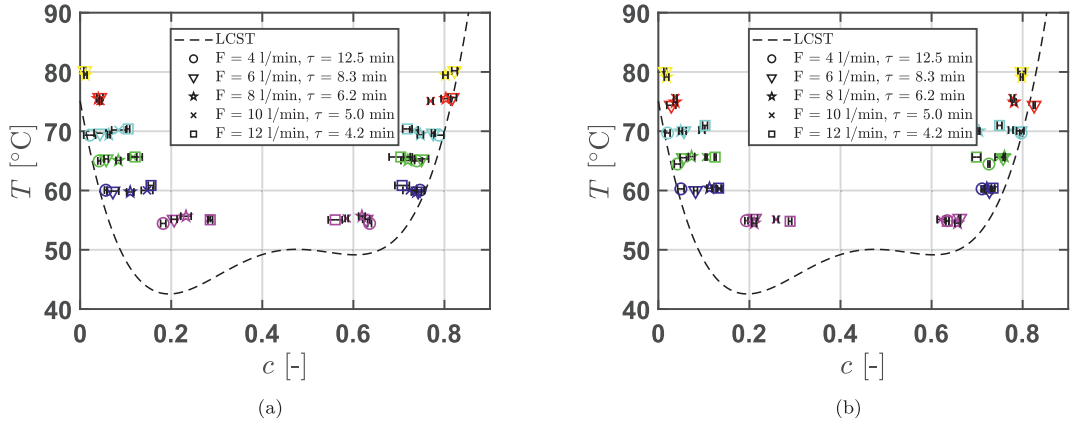

Fig. 9. Measured water-rich and polymer-rich phases concentrations compared with PAGB2000 LCST, at different T_{reg} and τ for Mesh #2 at: (a) c_{in} = 0.50; (b) c_{in} = 0.60.

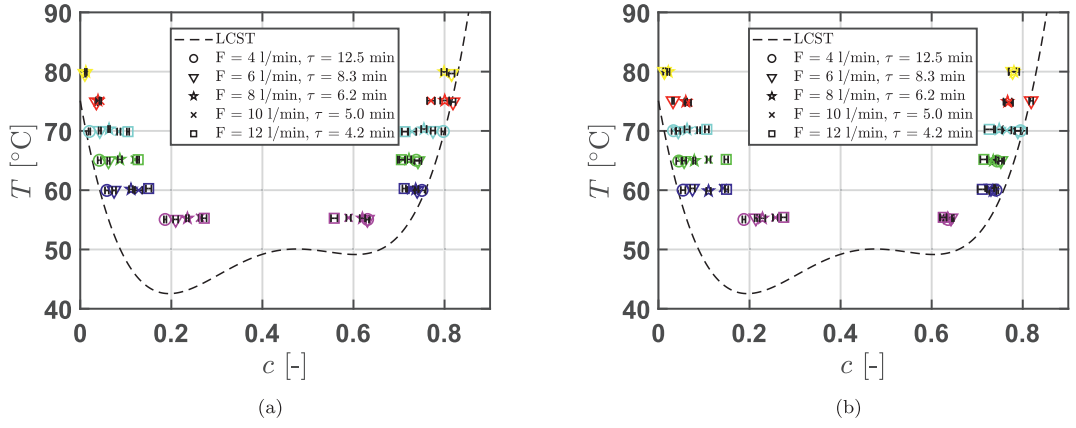

Fig. 10. Measured water-rich and polymer-rich phases concentrations compared with PAGB2000 LCST, at different T_{reg} and τ for Mesh #3 at: (a) c_{in} = 0.50; (b) c_{in} = 0.60.

3.2. Coalescer efficiency

Starting from the experimental results on concentrations, applying Eq. (3), the efficiency values are determined (Table 2) and analysed as function of T_{reg} and F at fixed c_{in}. The values reported show that the operating temperature of the coalescer, for the considered draw agent, should be above 70 °C which is consistent for the considered application (i.e., in advanced power cycles, heat is rejected from around 80 °C [3,12,13]). Moreover, for temperatures above 70 °C and flow-rates below 10 l/min, the efficiency can be above 95 %. No relevant differences can be noted between the three meshes.

Once calculated the efficiency, an analytical expression to predict the

Table 2
Efficiency values (ε) according to Eq. (3).

T_{reg}	F	M1				M2				M3			
		c_{in} [-]											
[°C]	[l/min]	0.30	0.40	0.50	0.60	0.30	0.40	0.50	0.60	0.30	0.40	0.50	0.60
55	4	51.8%	67.5%	75.0%	78.1%	51.1%	69.4%	73.0%	75.8%	61.0%	66.1%	71.6%	76.7%
	6	38.4%	54.0%	64.5%	73.6%	42.3%	59.1%	67.0%	72.3%	37.4%	55.2%	66.3%	71.6%
	8	36.1%	48.0%	57.2%	69.8%	33.0%	51.1%	60.7%	71.5%	33.5%	50.9%	60.3%	69.0%
	10	26.5%	40.3%	51.8%	65.1%	23.5%	46.7%	52.0%	63.2%	30.0%	46.6%	54.0%	63.6%
	12	17.5%	38.1%	48.2%	59.4%	26.9%	40.7%	48.1%	57.5%	23.2%	43.4%	51.9%	60.2%
60	4	99.5%	99.9%	98.3%	99.3%	95.2%	96.2%	97.0%	98.8%	96.9%	96.8%	96.6%	98.0%
	6	91.2%	92.6%	94.0%	95.0%	88.4%	91.8%	93.7%	93.1%	90.0%	91.4%	93.1%	94.1%
	8	83.1%	87.0%	87.1%	88.9%	75.5%	83.5%	85.5%	87.2%	76.9%	83.6%	84.9%	88.0%
	10	59.4%	76.6%	80.1%	84.5%	59.4%	76.5%	77.2%	83.4%	56.5%	76.1%	81.3%	82.0%
	12	56.0%	72.7%	78.6%	82.7%	55.2%	72.3%	74.8%	83.9%	51.4%	70.7%	76.3%	80.8%
65	4	100.0%	98.7%	96.8%	98.5%	100.0%	97.7%	93.3%	97.5%	100.0%	96.0%	96.7%	96.9%
	6	98.7%	93.5%	96.3%	95.2%	91.2%	92.4%	87.8%	94.9%	90.6%	92.4%	92.5%	94.8%
	8	91.4%	86.4%	88.1%	91.7%	87.9%	85.7%	80.7%	91.9%	86.6%	85.4%	87.1%	90.9%
	10	84.4%	79.7%	83.4%	88.9%	83.2%	79.8%	79.7%	86.4%	83.3%	79.2%	80.2%	85.4%
	12	76.8%	73.6%	78.8%	83.6%	76.6%	72.9%	97.7%	82.6%	74.7%	73.2%	78.7%	78.6%
70	4	99.1%	98.1%	98.7%	99.6%	100.0%	96.9%	95.8%	98.5%	99.7%	97.1%	98.5%	96.5%
	6	97.4%	93.9%	93.5%	93.2%	98.3%	93.0%	95.2%	92.5%	95.9%	92.5%	93.7%	94.7%
	8	94.1%	89.2%	89.8%	93.6%	92.4%	88.6%	92.6%	93.6%	92.8%	87.7%	89.4%	91.3%
	10	89.6%	83.4%	85.2%	86.5%	86.4%	84.7%	95.3%	85.7%	85.1%	84.4%	85.3%	87.1%
	12	86.4%	77.9%	81.8%	86.6%	84.1%	77.4%	94.8%	84.6%	82.7%	77.3%	81.1%	84.0%
75	6	96.4%	95.7%	91.9%	95.5%	95.4%	94.4%	91.0%	95.4%	95.1%	94.9%	93.0%	94.7%
	8	95.5%	91.6%	94.0%	94.0%	94.7%	91.2%	98.0%	94.0%	93.7%	90.3%	92.2%	90.1%
	10	92.0%	90.8%	91.7%	94.1%	90.4%	89.2%	96.9%	94.2%	90.1%	90.6%	91.2%	89.2%
80	6	97.6%	98.1%	98.0%	97.9%	97.5%	97.2%	96.8%	97.5%	96.9%	97.5%	98.0%	97.8%
	8	97.1%	97.4%	98.0%	97.6%	96.6%	97.1%	81.6%	97.0%	96.4%	97.1%	97.6%	96.4%

coalescer performance as function of the inlet conditions is proposed. The selected analytical expression is an exponential function based on the efficiency model for mass-exchangers, reported in [35]:

$$\varepsilon = 1 - C_1(c_{in}) exp\left\{\frac{C_2(c_{in})}{\tau} - C_3(c_{in})T^*\right\}, \quad (5)$$

where τ (residence time) is expressed as V/F, and T^* is the dimensionless temperature defined as:

$$T^* = \frac{T_{reg} - LCST(c_{in})}{T_{max} - LCST(c_{in})}, \quad (6)$$

having fixed $T_{max} = 85$ °C to include all the regeneration temperatures measured and hence to have a dimensionless temperature (T^*) always included in the range $0 \div 1$. In Eq. (5), $C_1(c_{in})$, $C_2(c_{in})$ and $C_3(c_{in})$ are three fitting constants that depend on the initial solution concentration.

This expression accounts for the control variables of the coalescence process: regeneration temperature, residence time and initial concentration. Eventually, the proposed equation complies with the physics of the phenomenon and on a mathematical standpoint shows a monotonic trend and is asymptotic to 1 for the experimental domain considered.

A Matlab® code was specifically developed to fit the experimental measurements (900 in total) and determine the fitting constants.

The efficiency results are reported both as 3D charts (Figs. 11–13) for

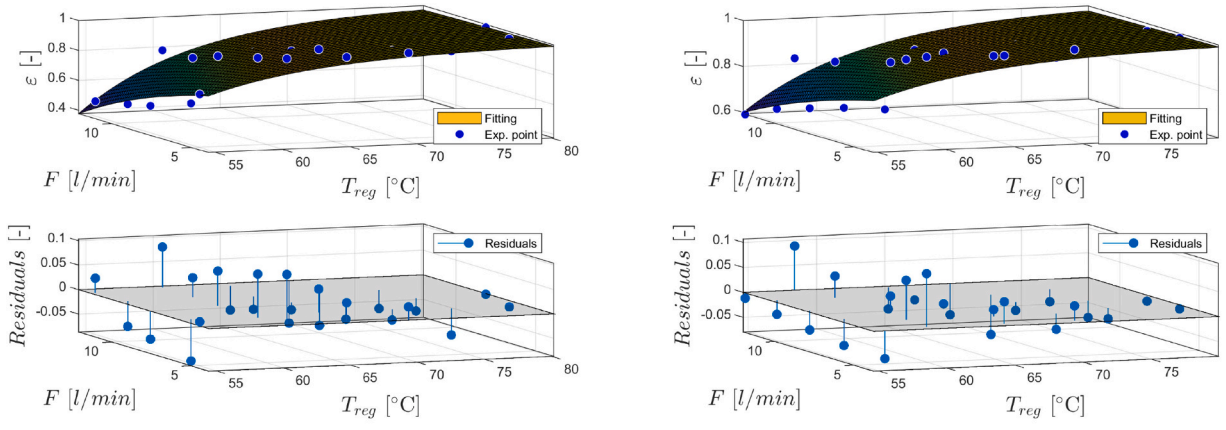

Fig. 11. Fitting surfaces (cf. Eq. (5)) and interpolation residuals for Mesh #1 at: (a) $c_{in} = 0.50$; (b) $c_{in} = 0.60$.

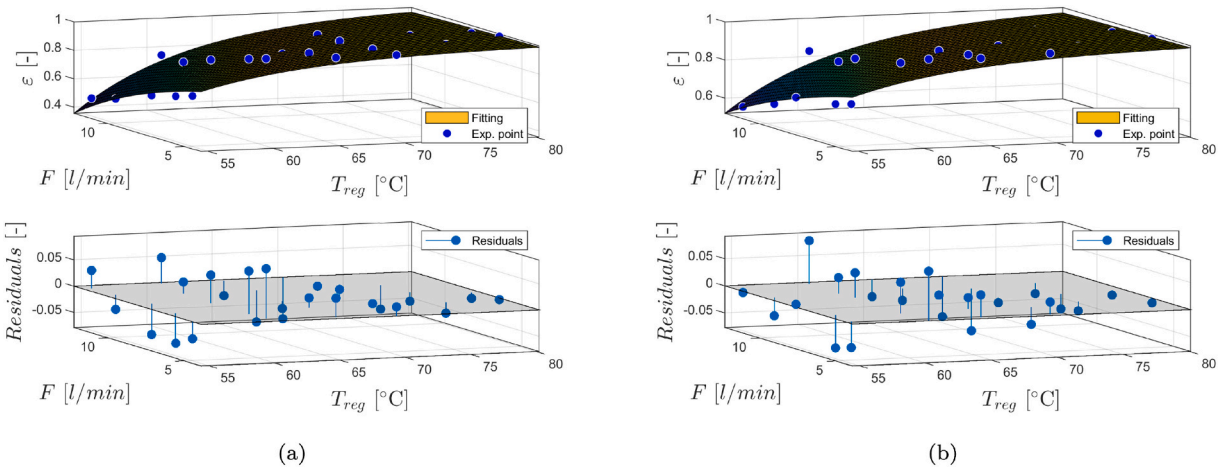

Fig. 12. Fitting surfaces (cf. Eq. (5)) and interpolation residuals for Mesh #2 at: (a) $c_{in} = 0.50$; (b) $c_{in} = 0.60$.

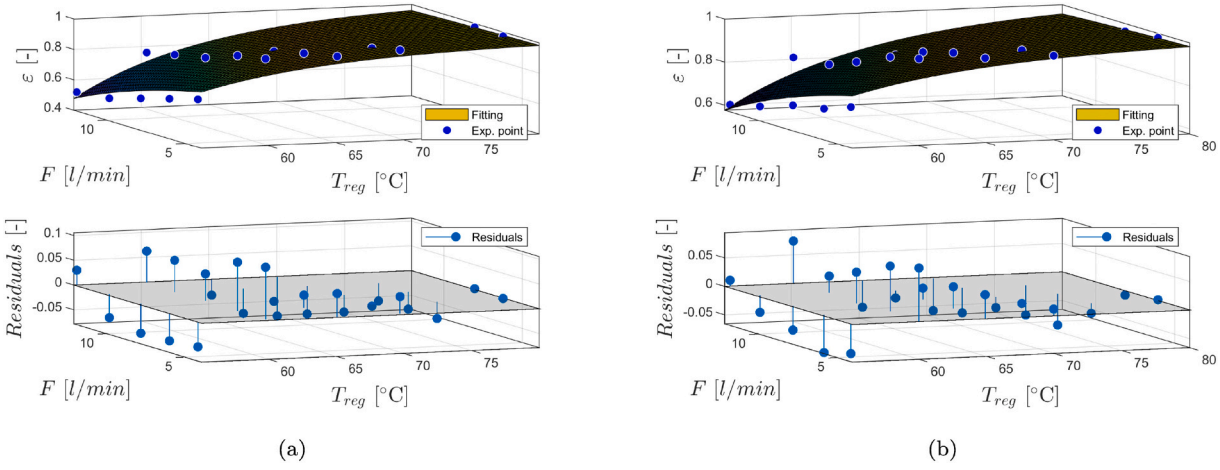

Fig. 13. Fitting surfaces (cf. Eq. (5)) and interpolation residuals for Mesh #3 at: (a) $c_{in} = 0.50$; (b) $c_{in} = 0.60$.

Table 3
Fitting surfaces parameters for each initial concentration for Mesh #1.

c_{in} [−]	C_1 [−]	C_2 [min]	C_3 [−]	R^2	*MRD* [%]	*MARD* [%]
0.30	1.46	4.76	7.19	0.93	−0.56	7.98
0.40	0.38	5.22	4.38	0.83	0.24	8.08
0.50	0.26	5.79	4.20	0.86	0.34	5.80
0.60	0.23	4.88	4.07	0.81	0.35	4.46

Table 4
Fitting surfaces parameters for each initial concentration for Mesh #2.

c_{in} [−]	C_1 [−]	C_2 [min]	C_3 [−]	R^2	*MRD* [%]	*MARD* [%]
0.30	1.34	4.69	6.04	0.92	−1.43	10.24
0.40	0.33	5.71	4.03	0.87	0.22	6.29
0.50	0.22	6.47	3.99	0.91	0.02	4.51
0.60	0.23	5.44	3.91	0.85	0.28	4.09

$c_{in} = 0.50$ and 0.60, and in tabular form (Tables 3–5) for all the initial concentrations tested.

The reliability of the fitting model here presented is guaranteed having for all the cases $R^2 > 0.80$ and both *MRD* and *MARD* included within the ±10%.

In addition, an analysis of the three coefficient constants is performed to develop an easy-to-use expression for coalescer efficiency. This analysis considers each mesh and involves plotting the constant

Table 5
Fitting surfaces parameters for each initial concentration for Mesh #3.

c_{in} [−]	C_1 [−]	C_2 [min]	C_3 [−]	R^2	*MRD* [%]	*MARD* [%]
0.30	1.07	4.43	5.34	0.91	−1.71	9.82
0.40	0.37	4.82	3.95	0.86	0.22	6.84
0.50	0.26	5.09	3.64	0.85	0.17	5.53
0.60	0.20	5.32	3.27	0.82	0.15	4.57

values against the initial concentrations (Fig. 14). In first approximation it results that C_1, C_2 and C_3 are independent of c_{in} and therefore the median value is chosen for each constant (for the three tested meshes) as summarized in Table 6.

The validity of the analysis is confirmed by a multi-variate-linear regression, that returns *p*-values on the initial concentration at least three-order of magnitude higher than for the other two variables (i.e., regeneration temperature and flow rate/residence time).

Hence the three efficiencies, starting from Eq. (5) can be written as:

$$\begin{cases} \varepsilon_{M1} = 1 - 0.32 exp\left\{\dfrac{5.05}{\tau} - 4.29T^*\right\} \\ \varepsilon_{M2} = 1 - 0.28 exp\left\{\dfrac{5.57}{\tau} - 4.01T^*\right\} \\ \varepsilon_{M3} = 1 - 0.32 exp\left\{\dfrac{4.96}{\tau} - 3.79T^*\right\} \end{cases} . \quad (7)$$

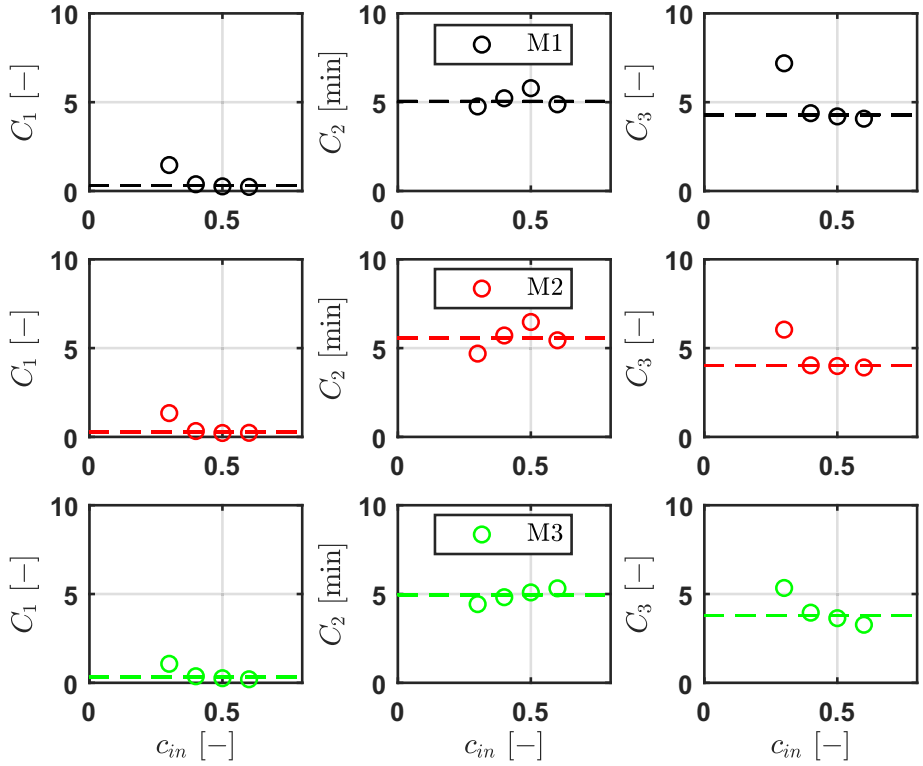

Fig. 14. Coefficients of the efficiency analytical expression (C_1, C_2 and C_3) vs. Initial concentration (c_{in}) for the three meshes tested.

Table 6
Median values of the three coefficients (C_1, C_2 and C_3) of the efficiency analytical expression for the three mesh tested.

Mesh [−]	C_1 [−]	MRD_{C_1} [%]	C_2 [min]	[%]	C_3 [−]	MRD_{C_3} [%]
M1	0.32	7.97	5.05	1.62	4.29	8.65
M2	0.28	12.12	5.57	−1.29	4.01	7.73
M3	0.32	1.43	4.96	−1.26	3.79	3.14

Having verified the independence of the initial concentration, it has to be checked how the metal meshes affect the coalescer efficiency. Hence, the constants are analysed as a function of the metal mesh density (ρ_M) (Fig. 15). It is determined that, due to the minimal variance observed in the values across the three meshes, the mean value can be assumed as representative.

Eventually, the final efficiency expression reads as:

$$\varepsilon = 1 - 0.31 exp\left\{\frac{5.19}{\tau} - 4.03T^*\right\}, \tag{8}$$

depending only on the residence time (i.e., flow rate and coalescer dimensions), and the dimensionless temperature (i.e., regeneration temperature and polymer selected through the LCST).

Although this is not the most general situation, in our experimental condition it is not surprising that the efficiency curves of the 3 meshes collapse in just one; since, as shown in Figs. 8–10, the concentrations of both water-rich and polymer-rich phases are very close to the LCST curve (i.e., to the asymptotic values they may reach) regardless the mesh considered. Hence, the ability of the 3 meshes to separate the two phases is similar which, in turn, leads to the same efficiency. Eventually, in the authors' opinion, this may be mainly related to two reasons: (i) the coalescer volume is very large, which induces high residence times, and (ii) having the draw agent thermo-responsive characteristics, it is likely to separate more as a result of the temperature than as a result of the mesh geometry. Further investigations in these directions are deserved.

4. Conclusions

This study focused on characterizing the efficiency of a coalescer used for liquid-liquid separation in a Forward Osmosis application. The coalescer minimizes the energy consumption for separating a water rich stream from a draw agent when thermo-responsive materials are adopted. Here, a thermo-responsive polymer (i.e., PAGB2000) was selected to be tested in accordance with previous studies which demonstrated its potentialities to produce pure water with low energy costs. Specifically, the experiments characterized the coalescer with

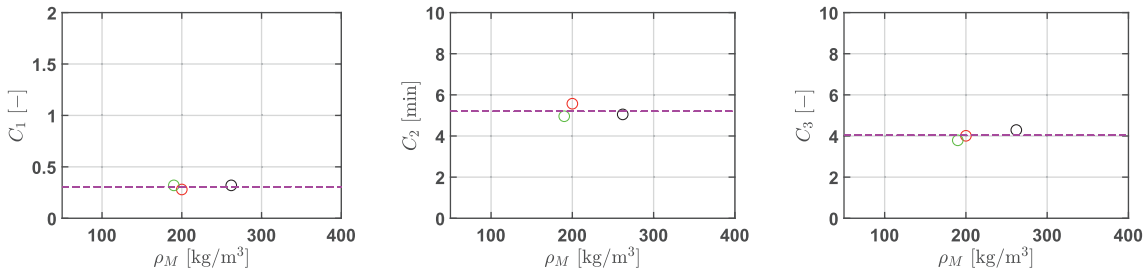

Fig. 15. Coefficients of the efficiency analytical expression (C_1, C_2 and C_3) vs. Mesh density (ρ_M).

three different metal meshes, at different operating conditions: initial solution concentrations, regeneration temperatures, flow rates. Results showed that this technology can be proficiently deployed in this context having separation efficiencies in most of the cases higher than 90% regardless both the initial concentration and the mesh selected. On the other hand, the efficiency strongly depends on both regeneration temperature and flow rate/residence time. Results are used to derive an expression (based on the efficiency of mass-exchangers) calibrated on experimental results to be used for the design of desalination plant facilities. Future works will focus on assessing the performance when using other thermo-responsive draw agents.

CRediT authorship contribution statement

Igor Matteo Carraretto: Writing – original draft, Resources, Methodology. **Davide Scapinello:** Validation, Investigation, Formal analysis. **Riccardo Bellini:** Validation, Investigation, Formal Analysis. **Riccardo Simonetti:** Conceptualization, Software. **Luca Molinaroli:** Writing – review & editing, Methodology, Conceptualization. **Luigi Pietro Maria Colombo:** Writing – review & editing, Supervision, Resources. **Giampaolo Manzolini:** Writing – review & editing, Supervision, Project administration, Funding acquisition, Conceptualization.

Declaration of competing interest

The authors declare that they have no known competing financial interests or personal relationships that could have appeared to influence the work reported in this paper.

Data availability

Data will be made available on request.

Acknowledgement

This project has been partly funded by the European Union's Horizon 2020 - Research and Innovation Framework Programme under grant agreement No. 101022686 (DESOLINATION). This study has been partly carried out within the NEST - Network 4 Energy Sustainable Transition (D.D. 1243 02/08/2022, PE00000021) and partly funded under the National Recovery and Resilience Plan (NRRP), Mission 4 Component 2 Investment 1.3, funded from the European Union - NextGenerationEU. This manuscript reflects only the authors' views and opinions, neither the European Union nor the European Commission can be considered responsible for them. We would like to thank Costacurta S.p.A.-VICO for providing the meshes to be tested.

Appendix A. Experimental results – supporting charts

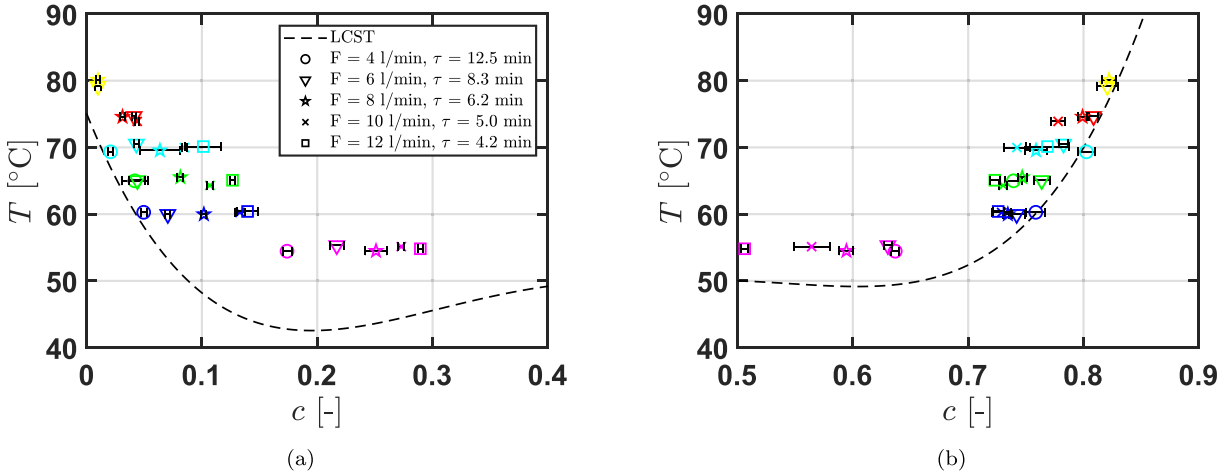

Fig. A.16. Zoom on measured (a) water-rich and (b) polymer-rich phases concentrations vs. PAGB2000 LCST, at different T_{reg} and τ for Mesh #1 and c_{in} = 0.50.

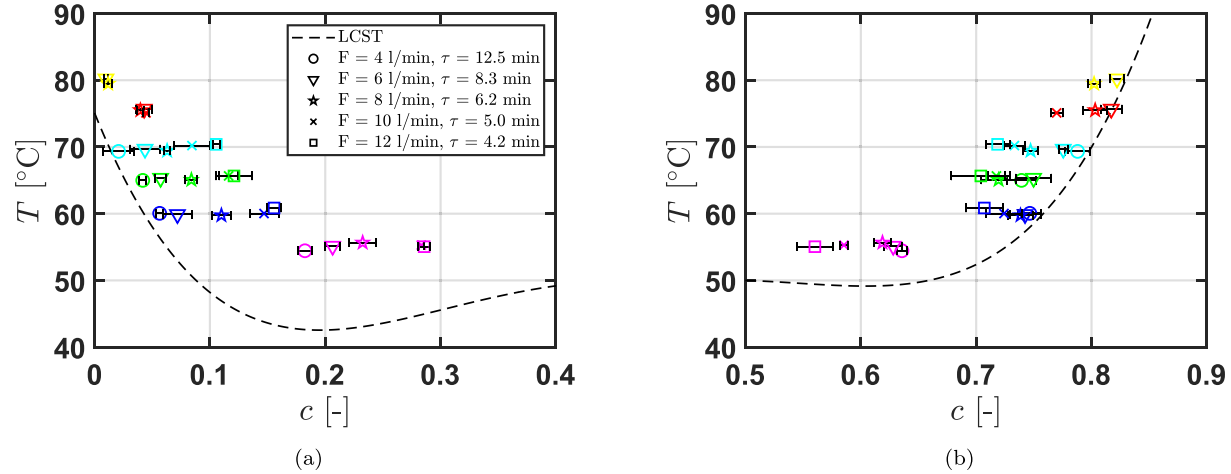

Fig. A.17. Zoom on measured (a) water-rich and (b) polymer-rich phases concentrations vs. PAGB2000 LCST, at different T_{reg} and τ for Mesh #2 and c_{in} = 0.50.

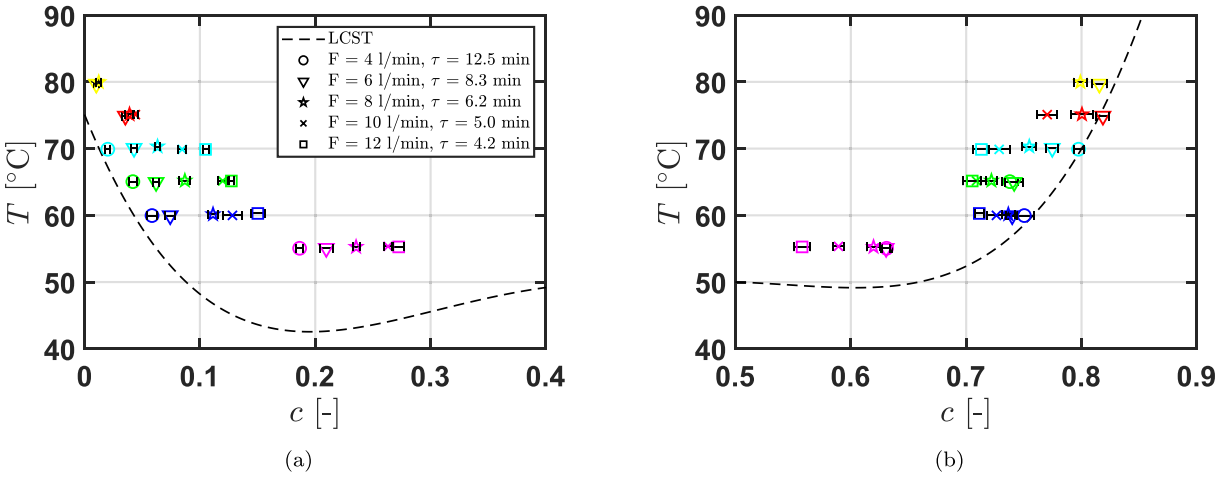

Fig. A.18. Zoom on measured (a) water-rich and (b) polymer-rich phases concentrations vs. PAGB2000 LCST, at different T_{reg} and τ for Mesh #3 and c_{in} = 0.50.

References

[1] UNESCO, United Nations World Water Development Report, https://www.unwater.org/publications/un-world-water-development-report-2023 (2023).

[2] M. Ayaz, M. Namazi, M. A. Ud Din, M. M. Ershath, A. Mansour, El Hadi M. Aggoune, Sustainable seawater desalination: current status, environmental implications and future expectations, Desalination 540. doi:https://doi.org/10.1016/j.desal.2022.116022.

[3] M. Doninelli, E. Morosini, G. Gentile, L. Putelli, G. Di Marcoberardino, M. Binotti, G. Manzolini, Thermal desalination from rejected heat of power cycles working with CO2-based working fluids in CSP application: a focus on the med technology, Sustain. Energy Technol. Assess. 60. doi:https://doi.org/10.1016/j.seta.2023.103481.

[4] K. Poirier, M. Lotfi, K. Garg, K. Patchigolla, E. Anthony, N. H. Faisal, V. Mulgundmath, J. K. Sahith, P. Jadhawar, L. Koh, T. Morosuk, N. Al Mhanna, A comprehensive review of pre- and post-treatment approaches to achieve sustainable desalination for different water streams, Desalination 566. doi:https://doi.org/10.1016/j.desal.2023.116944.

[5] A.B. Pouyfaucon, L. García-Rodríguez, Solar thermal-powered desalination: a viable solution for a potential market, Desalination 435 (2018) 60–69, https://doi.org/10.1016/j.desal.2017.12.025.

[6] AIP Publishing, Dynamic Thermal Analysis of an External Cylindrical Receiver in an Object-oriented Modelling Paradigm, Vol. 2445. doi:https://doi.org/10.1063/5.0085650.

[7] H. Truong-Ba, M.E. Cholette, G. Picotti, T.A. Steinberg, G. Manzolini, Sectorial reflectance-based cleaning policy of heliostats for solar tower power plants, Renew. Energy 166 (2020) 176–189, https://doi.org/10.1016/j.renene.2020.11.129.

[8] M. Qasim, N.A. Darwish, S. Sarp, N. Hilal, Water desalination by forward (direct) osmosis phenomenon: a comprehensive review, Desalination 374 (2015) 47–69, https://doi.org/10.1016/j.desal.2015.07.016.

[9] M. Amjad, J. Gardy, A. Hassanpour, D. Wen, Novel draw solution for forward osmosis based solar desalination, Appl. Energy 230 (2018) 220–231, https://doi.org/10.1016/j.apenergy.2018.08.021.

[10] Q. Long, Y. Jia, J. Li, J. Yang, F. Liu, J. Zheng, B. Yu, Recent advance on draw solutes development in forward osmosis, Processes 6 (9) (2018) 165, https://doi.org/10.3390/pr6090165.

[11] Desolination Project. https://www.desolination.eu/, 2021.

[12] E. Morosini, A. Ayub, G. di Marcoberardino, C. M. Invernizzi, P. Iora, G. Manzolini, Adoption of the CO2 + SO2 mixture as working fluid for transcritical cycles: a thermodynamic assessment with optimized equation of state, Energy Convers. Manag. 255. doi:https://doi.org/10.1016/j.enconman.2022.115263.

[13] G. Di Marcoberardino, E. Morosini, D. Di Bona, P. Chiesa, C. Invernizzi, P. Iora, G. Manzolini, Experimental characterisation of CO2 + C6F6 mixture: thermal stability and vapour liquid equilibrium test for its application in transcritical power cycle, Appl. Therm. Eng. 212. doi:https://doi.org/10.1016/j.applthermaleng.2022.118520.

[14] R. Colciaghi, R. Simonetti, L. Molinaroli, M. Binotti, G. Manzolini, Levelized cost of water assessment for small-scale desalination plant based on forward osmosis process, Energy Convers. Manag. 271. doi:https://doi.org/10.1016/j.enconman.2022.116336.

[15] G. Gentile, G. Picotti, M. Binotti, M. E. Cholette, G. Manzolini, A comprehensive methodology for the design of solar tower external receivers, Renew. Sust. Energ. Rev. 193. doi:https://doi.org/10.1016/j.rser.2023.114153.

[16] L. Zhang, X. Sun, S. Wu, A comprehensive review of responsive draw solutes in forward osmosis: categories, characteristics, mechanisms and modifications, Desalination (2024) 117676, https://doi.org/10.1016/j.desal.2024.117676.

[17] J.R. McCutcheon, M. Elimelech, Influence of concentrative and dilutive internal concentration polarization on flux behavior in forward osmosis, J. Membr. Sci. 284 (1–2) (2006) 237–247, https://doi.org/10.1016/j.memsci.2006.07.049.

[18] D. Zhao, P. Wang, Q. Zhao, N. Chen, X. Lu, Thermoresponsive copolymer-based draw solution for seawater desalination in a combined process of forward osmosis and membrane distillation, Desalination 348 (2014) 26–32, https://doi.org/10.1016/j.desal.2014.06.009.

[19] I. Petrinic, N. Jancic, R.D.J. van Vuuren, H. Buksek, Commercial thermo-responsive polyalkylene glycols as draw agents in forward osmosis, Desalination 582 (2024) 117576, https://doi.org/10.1016/j.desal.2024.117576.

[20] J.-J. Kim, H. Kang, Y.-S. Choi, Y.A. Yu, J.-C. Lee, Thermo-responsive oligomeric poly (tetrabutylphosphonium styrenesulfonate) s as draw solutes for forward osmosis (FO) applications, Desalination 381 (2016) 84–94, https://doi.org/10.1016/j.desal.2015.11.013.

[21] Y. Zhong, X. Feng, W. Chen, X. Wang, K.-W. Huang, Y. Gnanou, Z. Lai, Using ucst ionic liquid as a draw solute in forward osmosis to treat high-salinity water, Environ. Sci. Technol. 50 (2) (2016) 1039–1045, https://doi.org/10.1021/acs.est.5b03747.

[22] A.Z. Haddad, A.K. Menon, H. Kang, J.J. Urban, R.S. Prasher, R. Kostecki, Solar desalination using thermally responsive ionic liquids regenerated with a photonic heater, Environ. Sci. Technol. 55 (5) (2021) 3260–3269, https://doi.org/10.1021/acs.est.0c06232.

[23] Y. Cho, H. Kang, Thermosensitive magnetic ionic liquids with different heterocyclic moieties as draw solutes for forward osmosis, Desalination 569 (2024) 117045, https://doi.org/10.1016/j.desal.2023.117045.

[24] Y. Cai, R. Wang, W.B. Krantz, A.G. Fane, et al., Exploration of using thermally responsive polyionic liquid hydrogels as draw agents in forward osmosis, RSC Adv. 5 (118) (2015) 97143–97150, https://doi.org/10.1039/C5RA19018E.

[25] Z. Pan, H. Guo, H. Yu, G. Wen, F. Qu, T. Huang, J. He, Sewage sludge ash-based thermo-responsive hydrogel as a novel draw agent towards high performance of water flux and recovery for forward-osmosis, Desalination 512 (2021) 115147, https://doi.org/10.1016/j.desal.2021.115147.

[26] G. Gwak, B. Jung, S. Han, S. Hong, Evaluation of poly (aspartic acid sodium salt) as a draw solute for forward osmosis, Water Res. 80 (2015) 294–305, https://doi.org/10.1016/j.watres.2015.04.041.

[27] Q. Ge, G.L. Amy, T.-S. Chung, Forward osmosis for oily wastewater reclamation: multi-charged oxalic acid complexes as draw solutes, Water Res. 122 (2017) 580–590, https://doi.org/10.1016/j.watres.2017.06.025.

[28] A. Inada, K. Yumiya, T. Takahashi, K. Kumagai, Y. Hashizume, H. Matsuyama, Development of thermoresponsive star oligomers with a glycerol backbone as the draw solute in forward osmosis process, J. Membr. Sci. 574 (2019) 147–153, https://doi.org/10.1016/j.desal.2021.115311.

[29] A. Inada, K. Kumagai, H. Matsuyama, Effect of the molecular weights of thermoresponsive polyalkylene glycol draw solutes on forward osmosis performance, Sep. Purif. Technol. 252 (2020) 117462, https://doi.org/10.1016/j.seppur.2020.117462.

[30] R. Colciaghi, R. Simonetti, L. Molinaroli, M. Binotti, G. Manzolini, Potentialities of thermal responsive polymer in forward osmosis (FO) process for water desalination, Desalination 519 (2021) 115311, https://doi.org/10.1016/j.desal.2021.115311.

[31] S. Mokhatab, W.A. Poe, J.Y. Mak, Handbook of Natural Gas Transmission and Processing: Principles and Practices, 3rd Edition, Gulf professional publishing, 2018.

[32] TREVI Systems, FO Desalination System Using Inversely Soluble Copolymer Diol Draw Solution, in: https://www.trevisystems.com/technology/system-process, 2015.

[33] M. Ahmed, R. Kumar, B. Garudachari, J.P. Thomas, Performance evaluation of a thermoresponsive polyelectrolyte draw solution in a pilot scale forward osmosis seawater desalination system, Desalination 452 (2019) 132–140, https://doi.org/10.1016/j.desal.2018.11.013.

[34] I.M. Carraretto, V. Ruzzi, F. Lodigiani, R. Colciaghi, R. Simonetti, S. Buzzaccaro, L. Molinaroli, L.P.M. Colombo, R. Piazza, G. Manzolini, Characterization of the physical properties of the thermoresponsive block-copolymer PAGB2000 and numerical assessment of its potentialities in forward osmosis desalination, Polym. Test. 128 (2023) 108238, https://doi.org/10.1016/j.polymertesting.2023.108238.

[35] R.E. Treybal, Mass-transfer Operations, 3rd edition, McGraw-Hill Chemical Engineering Series, McGraw-Hill, New York, 1980.